Synthesis of Perfectly Oriented and Micrometer-Sized $MAPbBr_3$ Perovskite Crystals for Thin Film Photovoltaic Applications

Nadja Giesbrecht,[1] Johannes Schlipf,[2] Lukas Oesinghaus,[2] Andreas Binek,[1] Thomas Bein,[1] Peter Müller-Buschbaum,[2,] Pablo Docampo[1,]**

[1] Department of Chemistry and Center for NanoScience (CeNS), University of Munich (LMU), Butenandtstr. 11, 81377 Munich, Germany

[2] Lehrstuhl für Funktionelle Materialien, Physik-Department, Technische Universität München, James-Franck-Str. 1, 85748 Garching, Germany

AUTHOR INFORMATION

Corresponding Author

*E-mail: Pablo.docampo@cup.lmu.de.

*E-mail: muellerb@ph.tum.de.

ABSTRACT. Wide band-gap perovskites such as methylammonium lead bromide are interesting materials for photovoltaic applications due to their potentially high open-circuit voltage. However, the fabrication of high quality planar films has not been investigated in detail for this material. We report a new synthesis approach for the fabrication of bromide based perovskite planar films based on the control of the deposition environment. We achieve dense layers with large and perfectly oriented crystallites of 5-10 microns in size. Our results show that large crystal sizes can only be achieved for smooth ITO substrates, whereas lateral perovskite crystal growth is limited for the rougher FTO substrates. We additionally correlate photocurrent and perovskite crystal properties in photovoltaic devices and find that this parameter is maximized for ordered systems with internal quantum efficiencies approaching unity. Hence, our work not only gives a new pathway to tune morphology and crystal orientation, but also demonstrates its importance for planar perovskite solar cells.

TOC GRAPHIC:

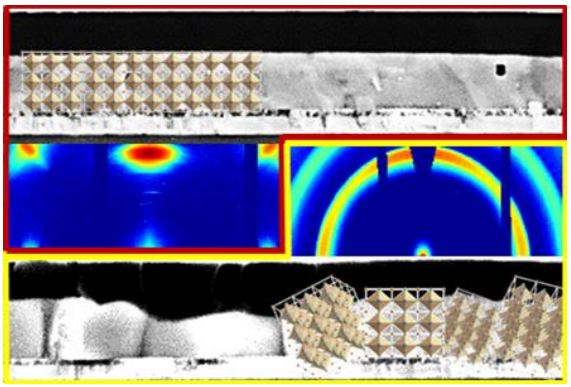

Perovskite based solar-cell development has been very impressive with power conversion efficiencies already exceeding 20 % after only a few years of development.[1] This fast development can be attributed to the excellent properties of the perovskite material, mainly its very high absorption coefficient[2] and long charge carrier diffusion length.[3-4] Furthermore, the perovskite material is easy to process from solution, with no high temperature steps required.[5] Although alternatives based on the exchange of iodide for bromide are interesting for applications in multijunction and photoelectrochemical devices, their fabrication has not been studied in detail.[6-9] Bromide-based compounds are interesting since they exhibit a wider bandgap of approximately 2.3 eV and thus can achieve much higher values compared to the iodide counterpart.[6, 8]

To date, the most efficient devices employing methylammonium lead bromide ($MAPbBr_3$) utilize a mesoscopic titania scaffold as the electron extraction layer.[6, 8] However, a planar architecture provides higher flexibility for device optimization, multijunction construction and thus can be employed in a wider variety of applications.[10-11] The main challenges for planar heterojunction solar cells, which we will focus on, are the perovskite film coverage, grain size and crystal orientation.[12]

Recent studies have highlighted the importance of the perovskite morphology, which determines to a large extent the performance of the final device.[13] In particular, further understanding of the crystallization processes has been the driving force behind the recent impressive device performance improvements in the iodide perovskite system.[14-17] Thus, a wide variety of deposition techniques has been developed, such as the fast deposition-crystallization procedure, vapor-assisted solution process, or the interdiffusion of solution-processed precursor stacking layers, respectively.[13, 18-19] To improve the solar cell performance in the bromide perovskite system, a similar improvement in morphology is expected to be necessary.

Recently, we have highlighted the importance of perovskite crystal orientation in the performance of the assembled devices.[20] A higher degree of preferential orientation of the crystallites in the perovskite film generally leads to higher device photocurrents and more reproducible solar cells overall.[20] Therefore, further understanding on the crystallization process for the bromide system will not only provide a path to enhanced performance with higher voltages of this system, but will also give insights applicable to other hybrid halide perovskite structures.

In this work, we introduce a new synthesis approach for $MAPbBr_3$ and incorporate this material into a planar device structure. We achieve extended control over crystallization such that the perovskite film exhibits densely packed and highly-ordered grains with crystallite sizes between 5 and 10 μm. We present the first grazing-incidence wide angle X-ray scattering (GIWAXS) investigation of the $MAPbBr_3$ perovskite and the highest orientation of the crystallites in a perovskite film ever reported for this family of materials. Such highly-ordered crystallites, in combination with the perovskite film quality in solar devices, maximize the charge collection efficiency leading to internal quantum efficiencies of over 95%.

In order to understand the impact of morphology and crystal orientation of methylammonium lead bromide based solar cells, we have prepared films via the state-of-the-art spin-coating the $PbBr_2$ and MABr precursors from γ-butyrolactone:dimethylsulfoxide solution (BD),[8] vapor-assisted solution process (VASP)[18] and via spin-coating from a lead acetate precursor, which we have termed controlled solvent drying (CSD). To deposit the perovskite via the state-of-the-art process, referred to as BD from here on, we spin-coated the perovskite from the precursor solution and added toluene during the spin-coating process with a subsequent heating step.[8] The deposition steps for the VASP technique are illustrated in the Supporting Information Figure SI1. In this case,

an initial lead bromide layer is deposited directly on TiO_2-coated ITO substrates and afterwards converted to the perovskite phase with methylammonium bromide (MABr) vapor.[18]

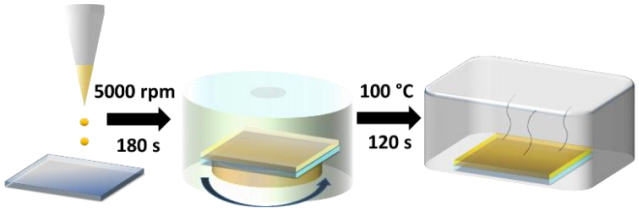

Figure 1: Schematic illustration of the perovskite-layer synthesis approach via CSD.

In Figure 1 we show a schematic illustration of the deposition-route via the CSD process. Our approach involves two stages wherein the solution of $Pb(Ac)_2$ and MABr precursors is spin-coated in a nitrogen-rich environment and is annealed under a glass cover. Here, we find that control of the solvent atmosphere during the whole crystallization process is crucial to maximize crystal size. In particular, films undergo gentle solvent annealing during the 3 minute spin-coating process as a result of the solvent coating the walls of the spin-coater. To achieve high-quality films, excess of solvent in the spin-coater must be removed between samples. Exposure to too much solvent or traces of alcoholic solvents such as methanol lead to secondary nucleation and inhomogeneous films, as shown in Supporting Information Figure SI5.

In Figure 2a, c, e we illustrate the morphology of the perovskite films prepared via VASP which has been shown in previous studies to achieve high performance when employed in solar cells.[7, 21] This morphology is comparable with the state-of-the-art films deposited on a mesoporous scaffold with full surface coverage and grain sizes of approximately 1 μm, and is similar to that achieved for the iodide system.[18, 21] On the other hand, films deposited via the CSD method are very smooth and also achieve full surface coverage with large crystals between 5 and 10 μm, as shown in

Figure 2 and Supporting Information Figures SI3 and SI4. We have also prepared films through the BD process, as shown in the Supporting Information Figure SI2. In this case, the crystal sizes are very small, in the range of 100 nm.[8]

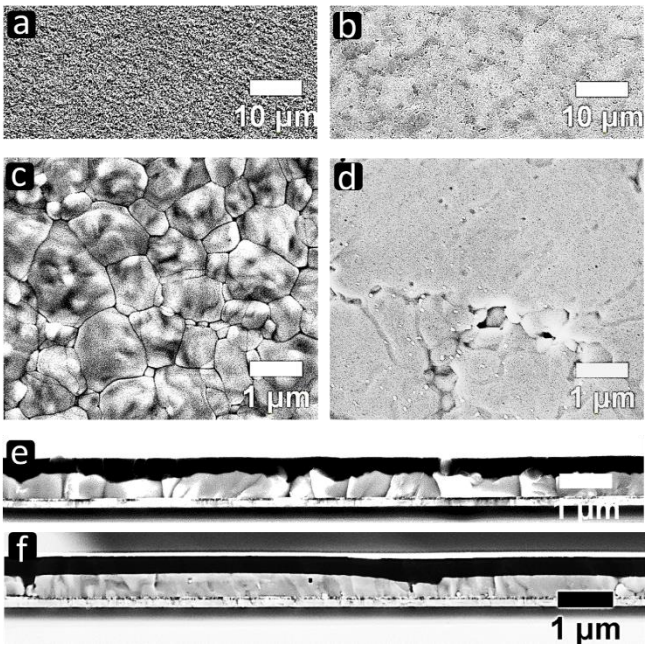

Figure 2: SEM top-view and cross-sectional images of $MAPbBr_3$ perovskite-film a, c, e) deposited on a TiO_2/ITO substrate by VASP, and b, d, f) deposited on TiO_2/ITO by spin-coating with a lead acetate precursor.

We attribute the full surface coverage and large grain size to our newly developed synthesis approach, which results in improved control over the crystallization of the perovskite. Low volatile solvents, such as dimethylformamide (DMF) are good candidates to grow large crystals at temperatures around 100 °C. However, achieving perovskite films with full surface coverage is challenging.[22-23] In our developed CSD method $Pb(Ac)_2$ and MABr react to form the perovskite structure and the excess organic components react to form methylammonium acetate, methylamine and acetic acid. All the expected organic components formed during the reaction are liquid at room

temperature which keep the films wet during the process. This in turn likely allows a certain degree of precursor mobility, and enables the very large and highly oriented crystal growth observed in the final films. Further evidence that this is the case is given by the structurally related formamidinium lead halide perovskite ($FAPbX_3$). Here, a solid formamidinium acetate salt is formed, and thus the films completely dry within the spincoating step. In turn this results in the formation of a non-continuous perovskite film with large voids between the crystals (see Supporting Information Figure SI3).

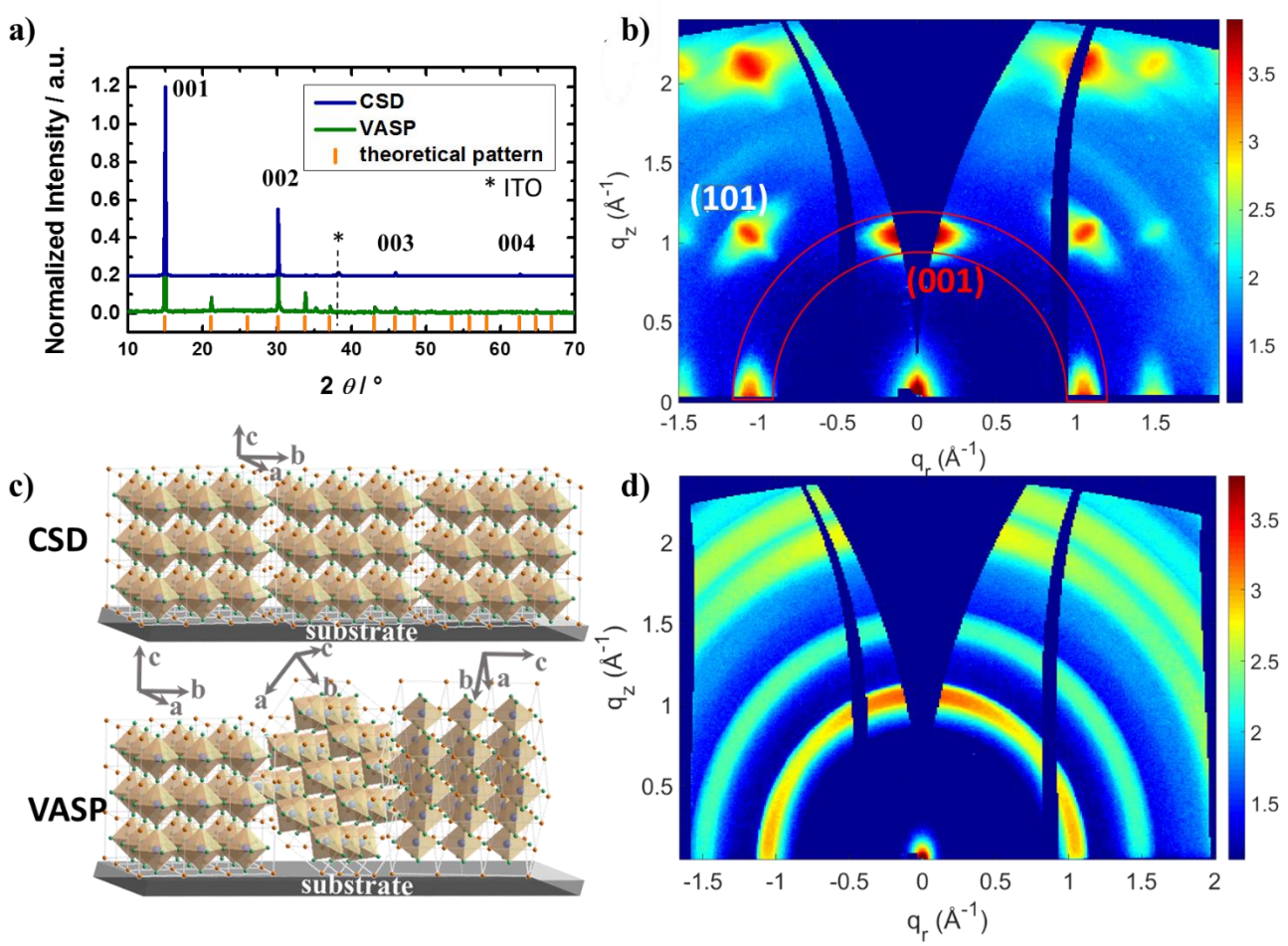

Figure 3: a) XRD patterns normalized to the reflex at 2 ϑ = 14.9 °, perovskite-film prepared via CSD and via VASP and the theoretical pattern, b) 2D GIWAXS patterns of the sample produced

via CSD ((001) and (101) peaks are marked in red and white, respectively. The data are corrected as outlined in the experimental section.), c) schematic illustration of the crystal orientation of the perovskite film prepared via CSD and disorder of the film prepared via VASP, d) 2D GIWAXS pattern of the sample produced via VASP.

To further investigate the crystalline quality of the films with the large domains, X-ray diffraction (XRD) experiments were performed for both CSD and VASP derived films. The X-ray patterns, shown in Figure 3a, confirm for both films a phase-pure $MAPbBr_3$ compound crystallized in the cubic $Pm\bar{3}m$ structure type. However, most of the reflections for the CSD sample are not present, which indicates a high degree of crystal orientation. A good tool to fully determine this parameter is grazing incidence wide-angle X-ray scattering (GIWAXS) which captures a two-dimensional slice through reciprocal space, allowing the reconstruction of the crystal structure and extraction of information on the orientation of the crystal planes from the azimuthal intensity distribution.[24-25] In Figure 3b and 3d we show GIWAXS data for VASP and CSD derived perovskite films. For VASP films, very homogeneous rings with no pronounced peaks are found. This implies no preferential orientation of the crystallites in the perovskite film. In contrast, films fabricated via the CSD process show very intense Bragg peaks and no rings. This implies that all crystallites are very well oriented with the {001} planes parallel to the glass substrate. This is remarkable for a thin polycrystalline film processed from solution. The orientation distribution is shown schematically in Figure 3c. We suggest that such a high degree of order is derived from the pre-crystallization step in the presence of a solvent layer on top. We note that a similar effect was observed for the iodide system when an ionic liquid was used to crystallize the perovskite.[26]

To correlate the effect of morphology and crystal orientation with the solar cell performance, we prepared devices with the developed perovskite layer in the standard device configuration, employing TiO_2 and Spiro-OMeTAD as the charge extraction layers, as shown schematically in Figure 4a. To exclude variations in the optical absorption of the films due to different perovskite film thicknesses, we have fixed this value for both techniques to 350 nm. The corresponding photovoltaic performance for perovskite films deposited via CSD and VASP is shown in Figure 4b, and the data are summarized in Table 1. In general, the performance of devices employing VASP-derived films is lower compared to those employing CSD-derived films. In Figure 4c, 4d and in Supporting Information Figure SI7 we show the distribution of the photovoltaic performance for the fabricated devices. The difference in device performance may arise from the different crystallization processes of the film leading to disparities in perovskite surface and in defect density. However, the VASP technique leads to the highest performance reported,[21] thus we expect the amount of defects to not be the major factor behind the variation in device performance.

Here, devices employing perfectly oriented perovskite films, derived via the CSD process, exhibit photocurrents between 6 and 7 $mAcm^{-2}$, which is twice the average value found for devices employing non-oriented perovskite crystals, prepared via the VASP process. We note that the theoretical limit for the short-circuit current extracted from light absorption measurements on devices is 7.15 $mAcm^{-2}$ which implies an internal quantum efficiency of over 95% (c.f. Figure SI6 in the Supporting Information).

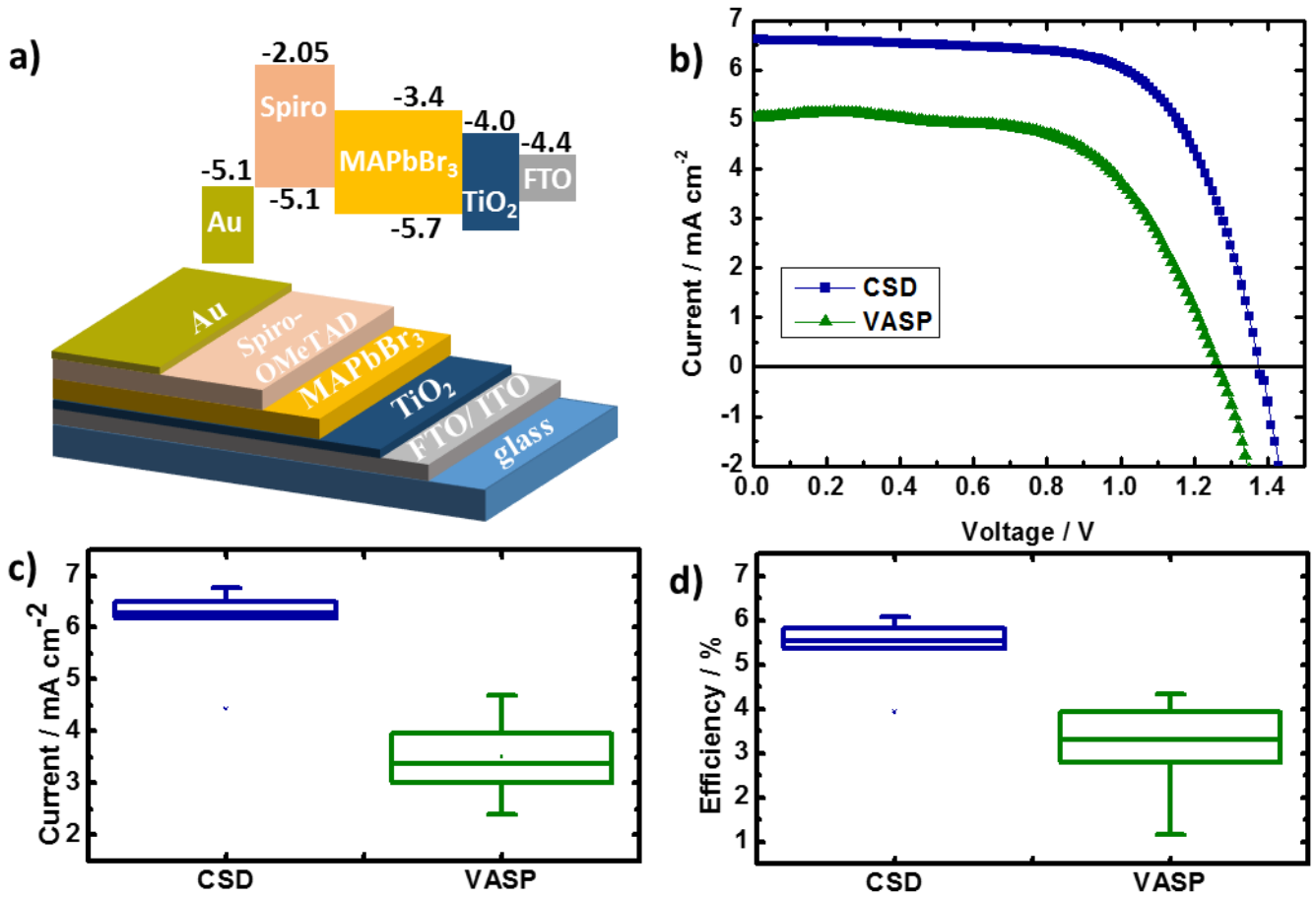

Figure 4: a) Scheme of the regular solar cell layout and energy diagram, b) J-V curves under AM 1.5 solar irradiation conditions for solar cell employing $MAPbBr_3$ derived from CSD or VASP processes, c) photocurrent and d) efficiency box plots of 20 devices employing VASP- or CSD-derived perovskite films. The edges of the box represent the 25/75 percentile, while the horizontal line represents the median value. Whiskers represent minimum and maximum values.

Table 1: Photovoltaic performance data of devices employing CSD- or VASP-derived perovskite films.

Method	V_{OC} / V	J_{SC} / mA cm^{-2}	FF / %	PCE / %
CSD	1.38	6.60	67	6.08
VASP	1.26	5.05	62	4.00

To further understand the differences in crystalline quality between films obtained from the CSD process and VASP derived films, we performed time-correlated single photon counting (TCSPC) to obtain the lifetime of the photoexcited species. Recent investigations showed that time resolved photoluminescence (PL) measurements yield not only important information about the diffusion length of the photoexcited species in the devices but also correlate with the perovskite layer morphology. In particular, larger crystals present narrower band gaps and longer lifetimes, which points towards a smaller radiative bimolecular recombination coefficient.[27] Our results presented in Figure SI6 agree with these findings, since we also observed a red shift of the steady-state PL maximum for the CSD-derived sample with respect to the BD- and VASP-derived sample. We also observed a slower bimolecular recombination process for films prepared with CSD, which is a strong indicator for good crystalline quality with fewer defects and lower disorder compared to BD- and VASP-derived films.[28-29]

The higher current for our CSD-derived films may be a result of either their larger crystal size, or their enhanced crystal order, as compared to those deposited via the VASP technique. In order to investigate this further, we have prepared devices with the rougher bottom contact FTO. This enhanced surface roughness hinders horizontal crystal growth and reduces the domain sizes in the perovskite layer, leading to crystal sizes comparable to those derived with the VASP approach, as

shown in Figure SI8 in the Supporting Information. However, these films maintain their high degree of orientation with the (001) plane parallel to the substrate, allowing us to discriminate between effects arising from the crystal size or the crystal orientation. We show histograms of all photovoltaic parameters in Figure SI9 in the Supporting information. Here, we observe that the short circuit current is not affected by the crystal size of the films, leading us to postulate that the degree of crystal order in the film is the parameter affecting the short circuit current. This may be a result of a lower number of defects at the grain boundaries as all neighboring crystals exhibit the same facets with the same orientation.

In summary, we have studied the role of morphology and crystal order in the photovoltaic performance of $MAPbBr_3$ deposited via three different deposition techniques. We developed a new fabrication method based on solvent drying with a halide-free lead precursor controlling the crystallization atmosphere. Here, the reaction of the precursors yields liquid organic by-products at RT which enable large crystal growth with perfectly oriented crystal planes parallel to the substrate as shown by GIWAXS measurements. Our results show that large crystal sizes can only be achieved for smooth ITO substrates, whereas perovskite films on FTO result in crystals limited to hundreds of nanometers due to the enhanced surface roughness which limits horizontal growth. In addition, we examined the role of perovskite crystallite orientation in planar heterojunction solar cells by comparing non-oriented VASP-derived films with our newly developed oriented CSD-derived films. We show that this perfect alignment of the cubic crystal planes parallel to the substrate of the CSD-derived film leads to a reproducible and high device performance. Additionally, we show enhanced short circuit currents approaching 7 $mAcm^{-2}$, their theoretical limit, compared to non-oriented VASP-derived perovskite films. The photocurrents generated in these devices correlate with the degree of crystal orientation rather than the crystal size. Thus, this

work demonstrates that crystal orientation and morphology are key parameters to maximize the short-circuit current and thus the performance of perovskite solar cells.

ASSOCIATED CONTENT

Supporting Information Available: Experimental section, statistics of photovoltaic performances and a more detailed description of the material with SEM images and XRD pattern included.

AUTHOR INFORMATION

Corresponding Author

*E-mail: Pablo.docampo@cup.lmu.de.

*E-mail: muellerb@ph.tum.de.

ACKNOWLEDGEMENTS

The authors acknowledge funding from the German Federal Ministry of Education and Research (BMBF) under the agreement number 01162525/1, the Bavarian Ministry of the Environment and Consumer Protection, the Bavarian Network "Solar Technologies Go Hybrid" (SolTech) and the DFG Excellence Cluster Nanosystems Initiative Munich (NIM). P.D. acknowledges support from the European Union through the award of a Marie Curie Intra-European Fellowship.

REFERENCES

(1) Yang, W. S.; Noh, J. H.; Jeon, N. J.; Kim, Y. C.; Ryu, S.; Seo, J.; Seok, S. I. High-Performance Photovoltaic Perovskite Layers Fabricated Through Intramolecular Exchange. *Science* **2015,** *348*, 1234-1237.

(2) De Wolf, S.; Holovsky, J.; Moon, S.-J.; Löper, P.; Niesen, B.; Ledinsky, M.; Haug, F.-J.; Yum, J.-H.; Ballif, C. Organometallic Halide Perovskites: Sharp Optical Absorption Edge and Its Relation to Photovoltaic Performance. *J. Phys. Chem. Lett.* **2014,** *5*, 1035-1039.

(3) Stranks, S. D.; Eperon, G. E.; Grancini, G.; Menelaou, C.; Alcocer, M. J. P.; Leijtens, T.; Herz, L. M.; Petrozza, A.; Snaith, H. J. Electron-Hole Diffusion Lengths Exceeding 1 Micrometer in an Organometal Trihalide Perovskite Absorber. *Science* **2013,** *342*, 341-344.

(4) Xing, G.; Mathews, N.; Sun, S.; Lim, S. S.; Lam, Y. M.; Grätzel, M.; Mhaisalkar, S.; Sum, T. C. Long-Range Balanced Electron- and Hole-Transport Lengths in Organic-Inorganic CH3NH3PbI3. *Science* **2013,** *342*, 344-347.

(5) Liu, D.; Kelly, T. L. Perovskite Solar Cells with a Planar Heterojunction Structure Prepared Using Room-Temperature Solution Processing Techniques. *Nat. Photon.* **2014,** *8*, 133-138.

(6) Edri, E.; Kirmayer, S.; Cahen, D.; Hodes, G. High Open-Circuit Voltage Solar Cells Based on Organic–Inorganic Lead Bromide Perovskite. *J. Phys. Chem. Lett.* **2013,** *4*, 897-902.

(7) Hanusch, F. C.; Wiesenmayer, E.; Mankel, E.; Binek, A.; Angloher, P.; Fraunhofer, C.; Giesbrecht, N.; Feckl, J. M.; Jaegermann, W.; Johrendt, D., et al. Efficient Planar

Heterojunction Perovskite Solar Cells Based on Formamidinium Lead Bromide. *J. Phys. Chem. Lett.* **2014,** *5*, 2791-2795.

(8) Ryu, S.; Noh, J. H.; Jeon, N. J.; Chan Kim, Y.; Yang, W. S.; Seo, J.; Seok, S. I. Voltage Output of Efficient Perovskite Solar Cells with High Open-Circuit Voltage and Fill Factor. *Energy Environ. Sci.* **2014,** *7*, 2614-2618.

(9) Noh, J. H.; Im, S. H.; Heo, J. H.; Mandal, T. N.; Seok, S. I. Chemical Management for Colorful, Efficient, and Stable Inorganic–Organic Hybrid Nanostructured Solar Cells. *Nano Lett.* **2013,** *13*, 1764-1769.

(10) Docampo, P.; Ball, J. M.; Darwich, M.; Eperon, G. E.; Snaith, H. J. Efficient Organometal Trihalide Perovskite Planar-Heterojunction Solar Cells on Flexible Polymer Substrates. *Nat. Commun.* **2013,** *4*, 2761.

(11) Bailie, C. D.; Christoforo, M. G.; Mailoa, J. P.; Bowring, A. R.; Unger, E. L.; Nguyen, W. H.; Burschka, J.; Pellet, N.; Lee, J. Z.; Gratzel, M., et al. Semi-Transparent Perovskite Solar Cells for Tandems with Silicon and CIGS. *Energy Environ. Sci.* **2015,** *8*, 956-963.

(12) Yin, W.-J.; Yang, J.-H.; Kang, J.; Yan, Y.; Wei, S.-H. Halide Perovskite Materials for Solar Cells: a Theoretical Review. *J. Mater. Chem. A* **2015**, 8926-8942.

(13) Xiao, M.; Huang, F.; Huang, W.; Dkhissi, Y.; Zhu, Y.; Etheridge, J.; Gray-Weale, A.; Bach, U.; Cheng, Y.-B.; Spiccia, L. A Fast Deposition-Crystallization Procedure for Highly Efficient Lead Iodide Perovskite Thin-Film Solar Cells. *Angew. Chem.* **2014,** *126*, 10056-10061.

(14) Im, J.-H.; Jang, I.-H.; Pellet, N.; Grätzel, M.; Park, N.-G. Growth of CH3NH3PbI3 Cuboids with Controlled Size for High-Efficiency Perovskite Solar Cells. *Nat. Nano* **2014,** *9*, 927-932.

(15) Jeon, N. J.; Noh, J. H.; Yang, W. S.; Kim, Y. C.; Ryu, S.; Seo, J.; Seok, S. I. Compositional Engineering of Perovskite Materials for High-Performance Solar Cells. *Nature* **2015,** *517*, 476-480.

(16) Jeon, N. J.; Noh, J. H.; Kim, Y. C.; Yang, W. S.; Ryu, S.; Seok, S. I. Solvent Engineering for High-Performance Inorganic–Organic Hybrid Perovskite Solar Cells. *Nat. Mater.* **2014,** *13*, 897-903.

(17) Ahn, N.; Son, D.-Y.; Jang, I.-H.; Kang, S. M.; Choi, M.; Park, N.-G. Highly Reproducible Perovskite Solar Cells with Average Efficiency of 18.3% and Best Efficiency of 19.7% Fabricated via Lewis Base Adduct of Lead(II) Iodide. *J. Am. Chem. Soc.* **2015,** *137*, 8696-8699.

(18) Chen, Q.; Zhou, H.; Hong, Z.; Luo, S.; Duan, H.-S.; Wang, H.-H.; Liu, Y.; Li, G.; Yang, Y. Planar Heterojunction Perovskite Solar Cells via Vapor-Assisted Solution Process. *J. Am. Chem. Soc.* **2013,** *136*, 622-625.

(19) Xiao, Z.; Bi, C.; Shao, Y.; Dong, Q.; Wang, Q.; Yuan, Y.; Wang, C.; Gao, Y.; Huang, J. Efficient, High Yield Perovskite Photovoltaic Devices Grown by Interdiffusion of Solution-Processed Precursor Stacking Layers. *Energy Environ. Sci.* **2014,** *7*, 2619-2623.

(20) Docampo, P.; Hanusch, F. C.; Giesbrecht, N.; Angloher, P.; Ivanova, A.; Bein, T. Influence of the Orientation of Methylammonium Lead Iodide Perovskite Crystals on Solar Cell Performance. *APL Mat.* **2014,** *2*, 081508.

(21) Sheng, R.; Ho-Baillie, A.; Huang, S.; Chen, S.; Wen, X.; Hao, X.; Green, M. A. Methylammonium Lead Bromide Perovskite-Based Solar Cells by Vapor-Assisted Deposition. *J. Phys. Chem. C* **2015,** *119*, 3545-3549.

(22) Xie, F. X.; Zhang, D.; Su, H.; Ren, X.; Wong, K. S.; Grätzel, M.; Choy, W. C. H. Vacuum-Assisted Thermal Annealing of CH3NH3PbI3 for Highly Stable and Efficient Perovskite Solar Cells. *ACS Nano* **2014**, 639–646.

(23) Zhang, W.; Saliba, M.; Moore, D. T.; Pathak, S. K.; Hörantner, M. T.; Stergiopoulos, T.; Stranks, S. D.; Eperon, G. E.; Alexander-Webber, J. A.; Abate, A., et al. Ultrasmooth Organic–Inorganic Perovskite Thin-Film Formation and Crystallization for Efficient Planar Heterojunction Solar Cells. *Nat. Commun.* **2015,** *6*, 6142.

(24) Saliba, M.; Tan, K. W.; Sai, H.; Moore, D. T.; Scott, T.; Zhang, W.; Estroff, L. A.; Wiesner, U.; Snaith, H. J. Influence of Thermal Processing Protocol upon the Crystallization and Photovoltaic Performance of Organic–Inorganic Lead Trihalide Perovskites. *J. Phys. Chem. C* **2014,** *118*, 17171-17177.

(25) Müller-Buschbaum, P. The Active Layer Morphology of Organic Solar Cells Probed with Grazing Incidence Scattering Techniques. *Adv. Mater.* **2014,** *26*, 7692-7709.

(26) Moore, D. T.; Tan, K. W.; Sai, H.; Barteau, K. P.; Wiesner, U.; Estroff, L. A. Direct Crystallization Route to Methylammonium Lead Iodide Perovskite from an Ionic Liquid. *Chem. Mater.* **2015,** *27*, 3197-3199.

(27) D'Innocenzo, V.; Srimath Kandada, A. R.; De Bastiani, M.; Gandini, M.; Petrozza, A. Tuning the Light Emission Properties by Band Gap Engineering in Hybrid Lead Halide Perovskite. *J. Am. Chem. Soc.* **2014,** *136*, 17730-17733.

(28) de Quilettes, D. W.; Vorpahl, S. M.; Stranks, S. D.; Nagaoka, H.; Eperon, G. E.; Ziffer, M. E.; Snaith, H. J.; Ginger, D. S. Impact of Microstructure on Local Carrier Lifetime in Perovskite Solar Cells. *Science* **2015,** *348*, 683-686.

(29) Wu, X.; Trinh, M. T.; Niesner, D.; Zhu, H.; Norman, Z.; Owen, J. S.; Yaffe, O.; Kudisch, B. J.; Zhu, X. Y. Trap States in Lead Iodide Perovskites. *J. Am. Chem. Soc.* **2015,** *137*, 2089-2096.